29th EPS Conference on Plasma Phys. and Contr. Fusion Montreux, 17-21 June 2002 ECA Vol. **26B**, P-5.074 (2002)

SOLUTION OF THE RESISTIVE TWO – FLUID WAVE EQUATIONS FOR ALFVÉNIC MODES IN SPHERICAL TOKAMAK PLASMAS

S.Cuperman[1] , C.Bruma[1,2] and K.Komoshvili[1,2]

[1] *Tel Aviv University,* [2] *The College of Judea and Samaria*

I. Introduction. Low Aspect Ratio Tokamak (LART) configurations represent a promising approach to thermonuclear fusion [1]. They require auxiliary non-ohmic power for heating, current drive and turbulent transport suppression. This paper provides the pre-requisite for the quantitative evaluation of these effects for pre-heated LARTs, namely the solution of the full wave equation and consequently, the consistent determination of the **global** electromagnetic field for Alfvènic modes in **inhomogeneous, magnetized, resistive, finite size plasmas** in the presence of **externally launched rf waves**. The "global" approach consists of the simultaneous treatment of the plasma-vacuum-external rf source-vacuum-metal wall configuration with the appropriate consideration of wave propagation, transmission, absorption and mode conversion. No simplifying approximations or small parameter expansions are used.

The problem is formulated in terms of the vector and scalar potentials ($\mathbf{A}$, $\mathbf{\Phi}$). Adequate boundary conditions at the vacuum - metallic wall interface and regularity conditions at the magnetic axis are enforced. A quite general,resistive, two-fluid based, dielectric tensor-operator able to describe the anisotropic plasma response — with full consideration of toroidicity, magnetic shear and non-circular cross section — is used; no geometrical limitations are imposed on it; the neo-classical conductivity is utilized.

The wave equation is solved by the aid of a computational algorithm based on the general $2\frac{1}{2}$D finite elements code PDE2D [2]. A full description of the analytical formulation and numerical procedures used will be presented elsewhere [3].

Illustrative solutions are obtained and presented for the low aspect ratio tokamak START ($R/a \approx 1.4$) [4]; the corresponding equilibrium configuration (magnetic field, plasma pressure and current) is reconstructed from experimental results and equatorial computations [5]. A sensitivity study to the antenna parameters (geometry, frequency and wave numbers) is also reported. Finally, as one of the possible applications of these results, the issueing ponderomotive forces and non-inductive current drive in a START-like device are calculated.

II. Solution of the full wave equations.

a. Effects of antenna geometry. In order to assess the influence of the antenna position and extension on the physics involved, we considered three different cases, namely (i) a $2\pi-$ concentric antenna, (ii) a two $\pi/2-$ angular extension antenna sections situated above and below the plasma cross section (UnD) and (iii) a low field side $\pm\pi/4$ extension antenna (LFS). In all three cases we used the same plasma parameters as well

as same antenna excitation frequency, wave numbers and current; thus, the total antenna currents corresponding to three cases satisfy the relations $4:2:1$. Illustrative computational results are presented in Fig.1 showing contours of $\Re A_\phi$ and $\Re\Phi$, Fig.2 showing the radial profiles of $\Re\Phi$ in the midplane of the cross section and Fig.3 showing the polar dependence of the radially integrated local power deposition and electromagnetic wave energy density. Thus, the similar structure of the solutions apparent in all three cases merely reflects the ratios $4:2:1$ corresponding to the actual currents of, respectively, 2π, UnD and LFS antennas used (Fig.1 and 2). This similarity obviously reflects the occurrence, in all three cases, of the same complex physical processes mentioned in Sec I. This is also evident in Fig.3 showing the polar dependence of the corresponding radially integrated local power deposition and electromagnetic energy density: here the square of the total antenna currents are involved and indeed one finds similar profiles with peak values satisfying, approximately, the relations $\textcircled{3} : \textcircled{2} : \textcircled{1} \cong 16:4:1$. Thus, not only in the midplane but over the entire domain, basically the same physics is involved. It appears, therefore, that given the plasma+wall equilibrium configuration and the physical parameters of the antenna (frequency, current and wave numbers), the structure of wavefield is almost insensitive to the polar location-extension of the antenna — thus reflecting the global character of the solution of the wave equation.

b. Effects of the pump frequency. To further the *understanding* (as well as a pre-requisite for subsequent *optimization* studies) of *the complex physics involved* we investigated the dependence on the pump frequency of the structures and relative intensities of the wavefields generated in the interaction of the antenna launched waves and the START-like plasma configuration. Fig.4 shows the dependence ot the total power deposition, P_{tot} for some 12 ω-values, between 5.5 and $8{\cdot}10^6$ rad/s. Thus, a strong increase occurs at a particular value, namely at $6.25{\cdot}10^6$ rad/s; specifically, one finds $\frac{P_{tot}(6.25\cdot10^6)}{P_{tot}(5.5\cdot10^6)} \simeq 20$, $\frac{P_{tot}(6.25\cdot10^6)}{P_{tot}(6.75\cdot10^6)} \simeq \frac{P_{tot}(6.25\cdot10^6)}{P_{tot}(8.00\cdot10^6)} \simeq 7$.

III. Illustrative applications. The solutions of the full wave equations obtained as described above can be used to evaluate a number of important quantities, e.g., the ponderomotive forces, the poloidal rotation velocities, the non-inductive current drive, the auxiliary non-ohmic plasma heating and the plasma turbulence and transport suppression barriers (see e.g. [6,7]). We here illustrate such evaluations.

a. Ponderomotive Forces. Fig.5 shows the magnetic surface averaged parallel components Lorentz, Hall, pressure associated and total ponderomotive forces for the pump frequency $\omega = 6.25\times10^6 rad/s$, corresponding to the peak value of the total power deposition. The Hall contribution is dominant while the pressure one – negligible.

b. Non–inductive current drive. We present in Fig.6 the magnetic surface averaged values of the non–inductive current drive component $< j_\phi >$ (top) and of the area

integrated toroidal component I_ϕ (bottom), for three relevant pump frequencies. Furthermore, in Fig.7, we show the same quantities, for three combinations of wave numbers and pump frequencies. **The variety of current drive profiles obtainable under conditions similar to those considered in the present work provides useful information for shaping them according to required stability conditions.**

In conclusion, the analytical + numerical algorithm developed can be reliably used for stability–optimization studies of any pre–heated LART–device; additional physical (e.g. kinetic, trapping) effects can be easily incorporated.

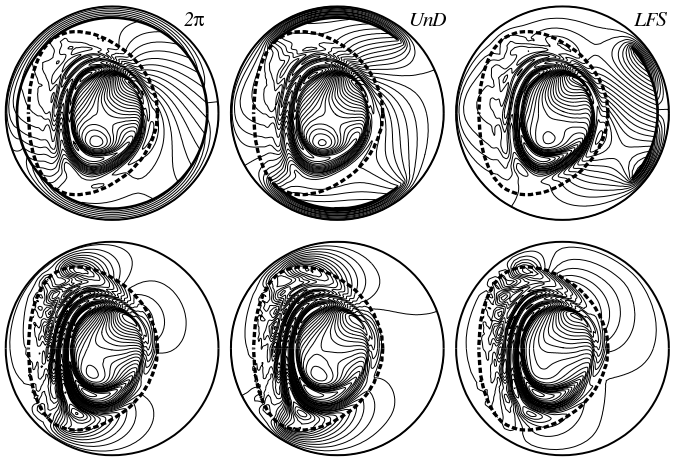

Fig.1 Contours of $\Re A_\phi$ (top) and $\Re\Phi$ (bottom) for three kinds of rf antenna geometry and localization, namely (from left to right) (3) 2π–circular, (2) two–$\pi/2$ angular extension sections situated above and below the plasma cross-section (UnD) and (1) the Reference case — $\pm 45°$ extension antenna about the midplane ($Z = 0$) and situated on the low field side (LFS). The antenna positions are indicated only on the top figures. In all three cases we used a pump frequency $\omega = 8 \cdot 10^6 rad/s$ and waves numbers $m = 1, n = 1$.

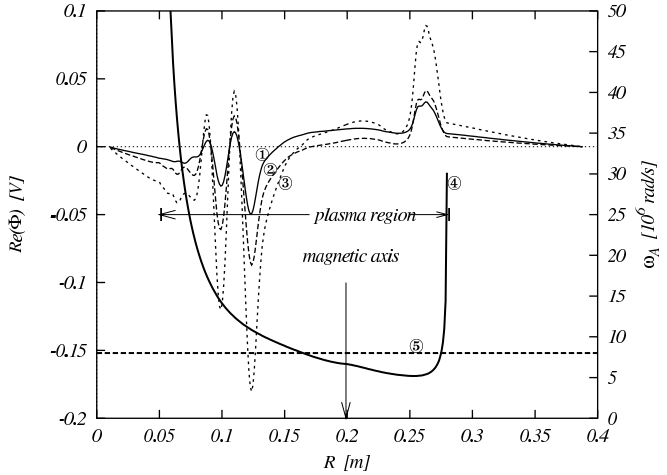

Fig.2 Radial profiles of the solutions $\Re\Phi$ in the midplane ($Z = 0$) for the antennas (1) — (3) described in the Fig.1. Also shown (in the lower part of the graph) are the approximate radial profiles of the Alfvèn frequency, (4) and the pump frequency, $\omega = 8 \cdot 10^6$ rad/s, (5).

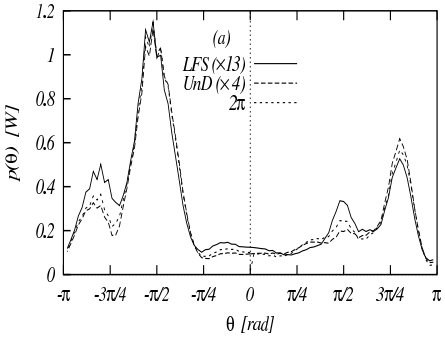

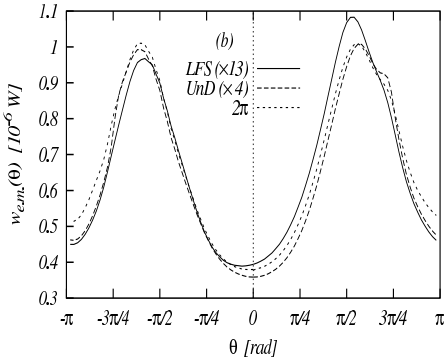

Fig.3 Polar (θ) dependence of the radially integrated local power deposition (top) and of the e.m. energy density (bottom) for the three types of antenna considered in Fig.1 and 2. The solid, dashed and dotted curves correspond, respectively to LFS, UnD and 2π circular antennas.

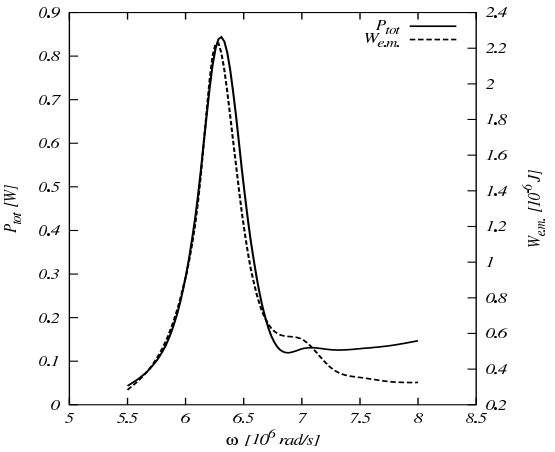

Fig.4 Dependence of the total power deposition and e.m energy on the pump frequency in the range $5.5 \leq \omega/(10^6 rad/s) \leq 8$; all other parameter are the same as in the Ref. case.

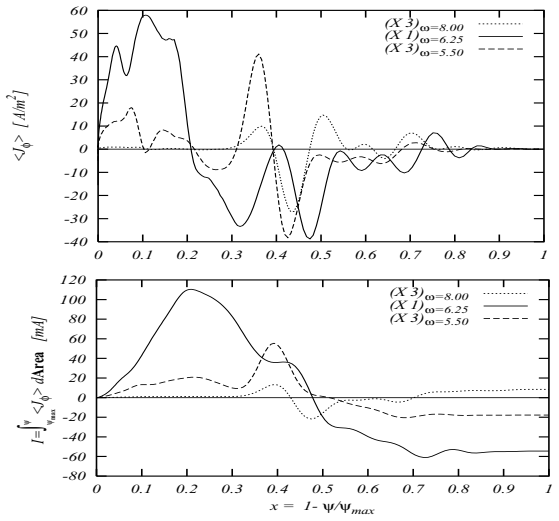

Fig.6 Top: Magnetic surface averaged toroidal current component $\langle j_\phi \rangle$, for three wave frequency values, namely, $\omega/10^6 rad \cdot s^{-1} = 8, 6.25$ and 5.5; bottom: corresponding integrated toroidal current component, $I(x) \equiv \int_0^x \langle j_\phi \rangle da$, with da — the area element.

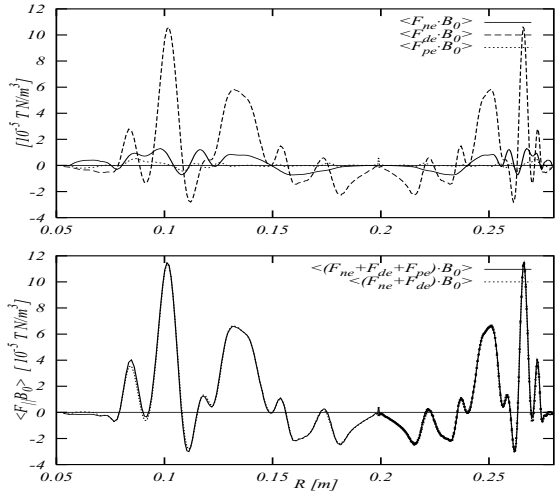

Fig.5 Magnetic surface averaged forces $\langle F_{e,l} \cdot B_0 \rangle$ ($l = L, H$ and the force associated with the wave pressure) (top) and $\langle \Sigma F_{e,l} \cdot B_0 \rangle$ (bottom) corresponding to the pump frequency $\omega = 6.25 \cdot 10^6 rad/s$

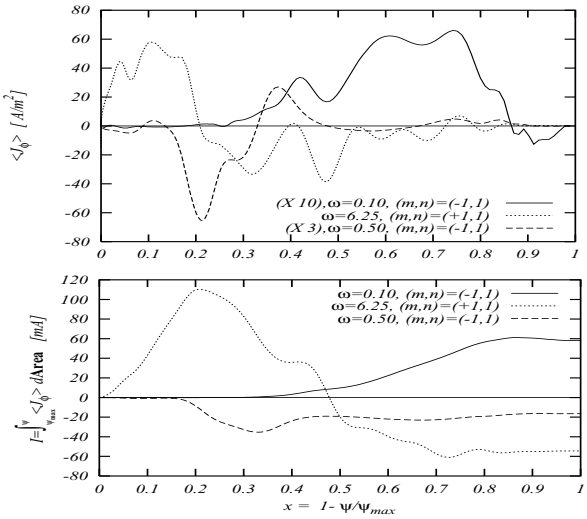

Fig.7 ψ-dependence of the magnetic surface averaged toroidal rf current drive components (top) and of the corresponding integrated current component, $I(x) \equiv \int_0^x \langle j_\phi \rangle \, da$ (bottom) for the indicated antenna parameters.

References

[1] Peng, Y.-K.M. 2000 *Phys. Plasmas* **7**, 1681.

[2] Sewell, G. 1993 *Advances in Engineering Software* **17** 105.

[3] Cuperman, S., Bruma, C. and Komoshvili, K., 2002 *in preparation for submission.*

[4] Sykes, A. 1994 *Plasma Phys. Contr. Fusion* **36**, B93.

[5] Wilson, H. R. 1994 "SCENE—Simulation of Self-Consistent Equilibria with Neoclassical Effects", *Fusion Depart.*, Culham Laboratory, Abingdon, UK.

[6] Burrell K. H., 1997 *Phys. Plasmas* **4**, 1499.

[7] Tsypin, V. S. et. al., 1995 *Phys. Plasmas* **7**, 2784.